First Demonstration of Laser Induced Breakdown Spectroscopy using Remote Handling for In-vessel Analysis of Tritiated and Activated JET Components

J. Likonen[1,*], S. Almaviva[2], R. Rayaprolu[3], R. Yi[3], I. Jepu[4], G. Sergienko[3], A. Widdowson[4], N. Jones[4], S. Atikukke[5], T. Dittmar[3], J. Karhunen[1], P. Gasior[6], Ch. Kawan[3], M. Sackers[3], S. Soni[5], E. Wüst[3], S. Brezinsek[3,7], J. Butikova[8], W. Gromelski[6], A. Hakola[1], I. Jõgi[9], P. Paris[9], J. Ristkok[9], P. Veis[5], and UKAEA RACE Team

[1]*VTT Technical Research Centre of Finland, PO Box 1000, FIN-02044 VTT, Finland*
[2]*ENEA, Diagnostics and Metrology Laboratory, Frascati, Italy*
[3]*Forschungszentrum Jülich GmbH, IFN-1 Plasma Physics, Jülich, Germany*
[4]*United Kingdom Atomic Energy Authority, Culham Campus, Abingdon, UK*
[5]*Comenius University, Faculty of Math., Physics and Informatics, Bratislava, Slovakia*
[6]*Institute of Plasma Physics and Laser Microfusion, Warsaw, Poland*
[7]*HHU Düsseldorf, Faculty of Mathematics and Natural Sciences, 40225 Düsseldorf, Germany*
[8]*University of Latvia, Institute of Solid State Physics, Riga, Latvia*
[9]*University of Tartu, Institute of Physics, Tartu, Estonia*

Abstract

The feasibility of laser-induced breakdown spectroscopy (LIBS) for measuring fuel retention was demonstrated for the first time in a tokamak operating with tritium using a remotely controlled *in-situ* application in JET. In JET as well as in future fusion reactors such as ITER and DEMO, thick co-deposited layers will be formed on the inner wall during extended plasma operations. Experiments in present-day fusion devices indicate that these layers consist of eroded plasma facing materials, various impurities and plasma fuel species such as deuterium and tritium. Accumulation of radioactive tritium in the reactor vacuum vessel is a particularly critical safety issue requiring active monitoring. LIBS is one of the few techniques available for monitoring the tritium content and the composition of co-deposited layers during maintenance breaks [1]. This paper will provide an overview of the LIBS experiment that was performed post DTE3 campaign, and D and H cleanup at JET in October 2024. 840 different spatial locations on the main wall and divertor area were investigated, with measurements of more than 100 laser pulses per location executed to ensure good depth resolution.

**Corresponding author address:* VTT, PO Box 1000, FI-02044 VTT, Finland.
**Corresponding author E-mail:* jari.likonen@vtt.fi

1. Introduction

In fusion devices, the plasma facing components (PFCs) are constantly bombarded by particles and energy flux from particle and power exhausts, edge localized modes (ELMs), major disruptions and energetic ion irradiation. These issues significantly impact the lifetime of the PFCs and machine availability. Therefore, the analysis and understanding of wall erosion processes, material transport and the retention of nuclear fuel are crucial activities for ITER and future nuclear fusion devices like DEMO. As a licensed nuclear facility, ITER must limit in-vessel tritium (T) retention to reduce the risks of potential release during accidents, with the inventory limit set at 1 kg. This limit includes 120 g of T trapped on the divertor cryopumps and 180 g of measurement uncertainty, so the maximum retention in the in-vessel components is set at 700 g [1]. To achieve this, an assessment of fuel retention in present and future fusion devices and power plants is necessary to improve understanding and procedures to meet regulatory requirements. Global retention measurements at ITER will be conducted using Pressure–Volume–Temperature-Composition (pVT-c) and calorimetry of T absorbed on uranium beds in the T-Plant [2]. However, these measurements do not provide information on where the tritium is locally trapped. Therefore, *in-situ* local measurements on PFCs are needed for a better understanding of temporal behaviour and spatial distribution of fuel retention. Among the possible *in-situ* techniques, laser-based techniques are promising candidates for first wall characterisation of a fusion device, providing in-vessel local fuel retention measurements for comparison with global fuel retention and with ex-vessel post-mortem measurements on retrieved PFCs.

Laser induced breakdown spectroscopy (LIBS) [3] experiments have been conducted on various fusion devices. In 2001 Summers et al. made *in-situ* measurements using the ex-situ LIDAR laser at JET [4]. Light was collected using a telescope, optical fibre and H_α and CIII interference filters. Discrimination between different hydrogen isotopes was not possible due to the 1 nm bandwidth of the filters. In 2007, Grisolia et al. reported laser-based applications for detritiation and provided the first proof of principle measurements using the ex-situ LIDAR laser at JET [5]. During these initial tests, the light observed was not, however, spectroscopically analysed, only its intensity was monitored. Semerok et al. [6] continued *in-situ* experiments using the ex-situ LIDAR laser at JET. They were able to distinguish and identify a number of analytical spectral lines (D, CII, CrI, and BeII) in the 400–600 nm spectral range when analysing inner divertor tile 1.

In 2009, Schweer et al. reported on an implementation for characterising the local wall surface of PFCs using laser-based techniques [7]. Subsequently, they further developed these techniques to diagnose the surface characteristics of the PFCs in TEXTOR tokamak [8]. In 2015, Xiao et al. [9] investigated the effect of toroidal magnetic field on carbon CII and CIII line intensities in TEXTOR tokamak. The Nd:YAG laser and the high-resolution spectrometer were located outside the vacuum vessel. Experiments conducted in TEXTOR revealed an increase in the spectral line emission in the presence of a magnetic field.

Almaviva et al. conducted multiple LIBS experiments on FTU. In Ref. [10] they investigated the impact of toroidal magnetic field on LIBS signals. The laser, collection optics and spectrometer were all located outside the vacuum vessel with the laser beam directed through a window to the bottom of the FTU vacuum vessel where the sample was mounted. The toroidal magnetic field was observed to enhance the intensities of Al and W lines, which aligns with the findings in Reference [9]. Maddaluno et al. [11] studied the influence of pressure on LIBS signals. The experiments were carried out in vacuum, as well as in argon and nitrogen atmospheres using a setup similar to Reference [10] but with the laser beam directed through an equatorial port to a toroidal limiter sector. LIBS measurements in nitrogen and argon atmospheres showed minimal presence and poorly resolved D_α and H_α lines, respectively. Due to time constraints, the optimisation of experimental parameters for nitrogen and argon was not as effective as in vacuum conditions. In 2020 Almaviva et al. [12] presented a new compact LIBS system mounted on the FTU robotic arm to demonstrate how the LIBS technique could be utilised at ITER using a multi-purpose deployer. The LIBS system used at JET is based on the design from Reference [12]. Experiments were conducted with samples placed in various positions of the FTU mock-up. In Reference [13] Almaviva et al. conducted LIBS experiments inside the FTU vacuum vessel using the robotic arm to sample several different areas within the vacuum vessel.

The LIBS technique has been extensively used in the EAST tokamak [14-22]. Experiments have been conducted to investigate the temporal and spatial dynamics of optical emission unde vacuum [14], the magnetic field effect on plasma plume [15], the analysis of co-deposition layers at different ambient pressures [16], the enhancement of the limit of detection by dual-LIBS [17], the optimisation of signal acquisition conditions [18], investigation of the history effect from successive ablation pulses [19], and model examination [20]. These investigations have provided insights into fuel retention and co-deposition of PFCs using the LIBS technique. The current design of the LIBS system at EAST is detailed in Reference [21]. In a recent

publication, Hu et al. [22] demonstrated a portable LIBS system that can be used in a manned entry to a tokamak. While this portable instrument cannot be used in future fusion reactors due to tritium concerns it may find applications in other areas.

Favre et al. reported on a measurement campaign conducted in the WEST tokamak using a novel LIBS device implemented on the Articulated Inspection Arm (AIA), demonstrating the feasibility of performing in situ LIBS experiments within the WEST tokamak [23]. The laser and spectrometer were located outside the vacuum vessel and the laser pulses were conveyed by an optical fibre. Hydrogen isotopes were not investigated in the WEST experiments due to their low abundance.

In JET-ILW, the main chamber consists of solid Be limiters that are in direct contact with the plasma, i.e. exposed to ion and charge exchange neutral (CX) fluxes as well as to ELMs and transient events. Additionally, in the main chamber, there are recessed limiters made of W-coated carbon fibre composite (CFC) tiles, and the main chamber inner wall is fully covered with Be-coated Inconel tiles. Both the recessed limiters and the inner wall are not in direct plasma contact, only exposed to CX flux. The divertor consists of W-coated CFC tiles and load bearing tiles made of solid W.

JET has operated with six dedicated tritium (T) or deuterium-tritium (DT) campaigns since 1991 recently summarised in [24]. JET operated from 2019 to 2023 without any intervention into the vessel and tile removal. In addition to deuterium and helium (He) campaigns, one tritium and two deuterium-tritium campaigns were performed in 2019-2023. After the last DT experiment (DTE3) in 2023 extensive tritium clean-up experiments were necessary to minimize the tritium inventory to acceptable levels before decommissioning [24]. The goal of the tritium clean-up was to reduce the tritium amount in the exhaust gases to 0.02% based on findings from the DTE2 clean-up campaign in 2022. This concentration was achieved after a six week period using various techniques: baking at 240 and 320 ^{o}C, Ion Cyclotron Wall Conditioning (ICWC), Glow Discharge Conditioning (GDC), Raised Inner Strike Point (RISP) plasma configuration, and finally high-power deuterium plasmas.

In 2023 a new diagnostic, Laser-Induced Desorption with detection by Quadrupole Mass Spectrometry (LID-QMS) was installed on JET [24]. The basic concept of LID-QMS diagnostics involves heating different spots on the first wall with intense laser radiation during plasma discharges and detect desorbed hydrogen isotopes using existing mass spectrometers in the vacuum vessel in-between discharges.

A more comprehensive application of LIBS for first wall analysis in fusion reactors, including implementations using robotic arms, is discussed in detail in the review paper [25] and the book chapter [26]. At the same time, the research was supported by laboratory LIBS experiments conducted on various tokamaks and specially prepared calibrated samples. This aspect of the investigation can be found in references [26-28].

The purpose of this paper is to present an overview of the LIBS experiment conducted in October 2024 at JET where a novel LIBS system was installed on the remote handling arm. LIBS is used to analyse material erosion and deposition in the main chamber and divertor, covering Be and W PFCs. Since detecting the fuel isotopes is crucial in ITER, the goal is also to accurately identify deuterium and tritium in the deposited layers by LIBS and distinguish them from hydrogen (protium). This study also involves measuring the qualitative depth profiles of various elements in samples taken from the JET ILW using LIBS and comparing the results with those obtained through post-mortem analysis techniques later.

2. Experimental

2.1 VTT campaign

Prior to the LIBS experiment at JET, test measurements were performed at VTT using the LIBS tool developed at ENEA [11,12]. The tool consisted of the LIBS enclosure equipped with a sub-nanosecond Nd:YAG laser and focusing optics, which was connected via a 20 m optical fibre to an Echelle type spectrometer (Aryelle 200) with a wide spectral range (200-760 nm). Samples, including those from JET limiters and divertor, were analysed for calibration-free LIBS and for calibration of the ablation rate. The prototype LIBS system is shown in Figure 1.

The main component of the LIBS tool is a Nd:YAG laser (Montfort Laser M-Nano laser), emitting at the fundamental wavelength of 1064 nm. Each pulse has a duration of 0.8–0.9 ns and the maximum output energy is 10 mJ/pulse. The pulse repetition rate of 2 Hz was chosen due to limitations by the camera of the Aryelle 200 spectrometer (LTB Lasertechnik Berlin GmbH). The laser beam had a Gaussian profile, and the resulting crater was partly ellipsoidal, likely due to the optics in the LIBS tool, with the major and minor axes measuring 0.6 and 0.4 mm, respectively.

The laser beam was directed using lenses 1 and 2, along with two 45° mirrors. The second mirror was a 45º incidence dielectric mirror with the highest reflectivity at a wavelength of

1064 nm and high transmission at shorter wavelengths. To focus the laser beam, a fused silica plano-convex lens (L3) with a 75 mm focal length was used. The focal point of the lens was a few millimeters inside the target to prevent the breakdown of atmospheric gas. The experiments were conducted at atmospheric pressure with an argon flow of 1 slm. The sample intended for analysis with LIBS was placed against a cone which facilitated the use of argon as the background gas inside the cone. This setup ensured the repeatability of the optical setup's focusing. To prevent beryllium and tritium contamination of the surrounding areas, the sample manipulator was placed inside a plexiglass cabinet.

The emission of the plasma plume was collected collinearly, perpendicular to the target surface, through lens 3 located inside the cone and the 45° dielectric mirror. It was then focused with lens 4 onto a 20-meter optical fibre with an active pure fused silica core diameter of 1.5 mm. This setup enabled the collection of emission light from the entire plasma plume. The other end of the fibre was attached to a fibre bundle that is split into seven outputs with an effective transmittance from 260 nm, allowing for the connection of multiple spectrometers and other diagnostic tools at JET to the fibre.

Wavelength calibration of the Aryelle spectra was conducted using an Hg calibration lamp within the 200–760 nm spectral range. The spectral sensitivity calibration was carried out using an Ocean Optics DH2000 deuterium-halogen lamp and the intensity was adjusted by modifying the camera gain function and gate width. For both calibrations, the fibre was disconnected from the LIBS enclosure and directly connected to the calibration lamp. As a result, the sensitivity curve did not include the optics inside the LIBS enclosure. However, the transmission of the final optical setup was determined using Zemax OpticsStudio [29] software and factored into the data analysis of the actual JET LIBS experiment.

Several JET samples were analysed during the LIBS experiments at VTT, including samples from the inner wall guard limiter (IWGL), outer wall poloidal limiter (WPL) and divertor exposed during the 2011-2016 ILW1-3 campaigns (see Fig. 2). The list of the analysed samples, along with the expected layer structure and exposure period, is provided in Table 1. This set of samples provided an overview of the erosion/deposition pattern inside the vacuum vessel for the subsequent LIBS experiment at JET. The JET ITER-like Wall (ILW) divertor typically consists of carbon fibre composites (CFC) tiles coated with a ~ 20 μm thick tungsten (W) layer over a thin molybdenum (Mo) interlayer designed to inhibit interaction between the carbon and the tungsten. In JET-ILW, divertor tile 5 is made of bulk tungsten and the vessel main chamber is made of bulk beryllium (Be), respectively. The CFC divertor tiles were cored into small-sized

samples with a diameter of 17 mm [30] and the castellated Be limiter tiles were sectioned into samples with a thickness of 10 mm [31].

2.2 JET campaign

JET operated continuously without any shutdowns and tile removal from 2019 to 2023, conducting three dedicated tritium (T) and deuterium-tritium (DT) campaigns during this period [23]. The last campaign, DTE3, took place in 2023, with a total of 359 g of tritium injected during the 100% T_2, DTE2 and DTE3 experiments. Tritium clean-up was carried out twice after these campaigns to reduce the production of 14 MeV neutrons from the DT nuclear reactions and preserve the lifetime budget for JET. The clean-up after the DTE2 campaign reduced the tritium amount in exhaust gases to 0.02% in hydrogen and low-power D plasmas [32,33].

The DTE3 clean-up campaign was optimised based on the results of the DTE2 clean-up, achieving a similar reduction in tritium concentration in exhaust gases to 0.02%. The clean-up process involved various techniques such as main chamber baking at 240°C and 320°C, ICWC, GDC and Raised inner Strike Point (RISP) plasma configuration decreasing the tritium concentration to ~0.1% [33]. Tritium concentration was monitored during the clean-up using the ratio of 14 MeV neutron data to 2.4 MeV neutron data (from DT and DD nuclear reactions respectively) as a proxy for tritium concentration. Subsequent high-power deuterium plasmas further reduced the tritium concentration to 0.02% [32,33]. As the clean-up progressed and data indicated that the tritium concentration was nearing 0.02%, several JET experiments in deuterium plasmas were conducted in between the cleaning sessions. Once the target tritium concentration was achieved, JET operations continued with experiments in deuterium plasmas. Throughout this period, tritium concentration was continuously monitored using neutron diagnostics.

Commissioning of the LIBS system continued at JET after the campaign at VTT leading up to the actual remote-handling LIBS experiment. The LIBS sub-nanosecond laser and optics were re-installed and aligned in the final LIBS enclosure. It was discovered that the final focusing lens inside the cone was contaminated, due to previously ablated material from the sample. A new cone design was created, resulting in a new cone with a smaller opening (reduced from 10 mm to 4mm in diameter). Several experiments were carried out to optimize the position of the final focusing lens using Zemax calculations to avoid reflections. The beam expander (L1 and L2) was also removed as it was causing deterioration in beam quality. The lens L3 inside the cone was switched to an uncoated lens for better transmission properties.

Additionally, a diaphragm was installed in front of the laser to prevent back-reflected light from entering the laser. The final LIBS setup is shown in Figure 3. Overall, the setup used at VTT was redesigned to improve focus and beam quality to meet the standards required at JET for measurements on the remote handling arm. One of the fibre outputs was connected to a high-resolution Littrow spectrometer [34] with a large etendue of 2.4×10^{-4} cm^2 s rad and a resolution of 0.03 nm at 500 nm. The spectrometer operated at distinct camera settings which were different from the Aryelle camera. Moreover, it was capable of distinguishing hydrogen isotopes at 656 nm. In addition to the Aryelle and Littrow spectrometers a third spectrometer (Avantes AvaSpec-ULS2048CL) was used during the LIBS experiments at JET. This compact spectrometer provides an overview spectrum in the wavelength range of 300-1100 nm.

Subsequently, the LIBS hardware was relocated from an optical lab at UKAEA to the JET torus hall and commissioned within the controlled area. Final calibration measurements were performed using H/D, D, Hg and W lamps for wavelength calibration as well as an Ulbricht sphere for radiometric calibration. The LIBS tool was mounted on the MASCOT arms (see Figure 4). The MASCOT telemanipulator robot [35] is a two-armed machine with back-drivable actuators and a large dexterous workspace in which each arm can operate within the full six degrees of freedom. The manipulator is remotely operated from a control room. All the spectrometers and photomultipliers were located outside the JET vacuum vessel.

The LIBS experimental campaign at JET utilising remote handling, was successfully conducted from October 2nd and to October 18th in double shifts. A total of 840 different spatial locations on the main wall and divertor area were investigated, with over 100 measurements taken per location to ensure good depth resolution. The distribution of locations in various areas of the JET vacuum vessel is detailed in Table 2. Tile 2XR9 of the Inner wall guard limiter (IWGL) from the centre of the limiter and the wide poloidal limiter (WPL) tile 4D13 also from the centre of the limiter were most extensively analysed to demonstrate the spatial resolution of the remote handling equipment and the LIBS setup. Figure 5 displays the analysed locations on WPL tile 4D13, with full scanning of odd numbered rows. The divertor area was also thoroughly, as depicted in Figure 6. Due to space constraints, the bottom of tile 3 and 7, as well as tile 6, could not be analysed. Remote areas of tile 4 and 6 were also inaccessible.

In addition to these analyses. some Inner wall protection (IWP) tiles were measured for calibration of the ablation rate. These tiles are situated in the plasma shadow shielding them from heavy erosion. IWP tile 428 contains sachet samples with a thin Be (2.5 μm) and W coating (50 nm), illustrated in Figure 7. In total, ~323000 laser shots were applied each

producing an Aryelle, Littrow and Avantes spectrum. The amount of data generated is substantial so advanced Matlab and machine learning algorithms will be utilised for batch processing of the spectra during the data analysis.

3. Results and Discussion

3.1 Fuel retention

Widdowson et al. [31,36] assessed the tritium (T) inventory in plasma facing components (PFC) during JET T and DT operations based on ex-situ post-mortem analyses during ILW3. The global D retention as a percentage of the injected fuel was determined to be ~0.2 % [36]. Recently updated calculations are presented in Table 3 (2nd column). A two order of magnitude reduction in 14 MeV neutron production (T content %) from the start to the end of clean-up was observed, resulting in T retention values divided by a factor of 100 after the clean-up. The inventory of T can also be estimated by using the total amount of T injected during DTE3 (2.15 x 10^{25} at [24]), the post-mortem analysis fuel retention of 0.2 % and the reduction in T retention by two orders of magnitude due to the clean-up. T injected during the T_2 and DTE2 can be neglected due to the clean-up after DTE2. When multiplying the T amount injected during DTE3 with the fuel retention, the efficiency of the clean-up and retained fraction of retention in the inner divertor (46.5 % [36]), and by dividing by the area of the inner divertor (8.73 m^2, [36]) we get a value of 2.3 x 10^{15} at/cm^2 for the inner divertor which agrees well with the corresponding number in Table 3.

Calculating D retention is somewhat challenging due to the clean-up campaigns following DTE2 and DTE3 which also included ICWC and GDC operations. ICWC and GDC primarily focused on the main chamber wall retention, with ICWC being ineffective for divertor cleaning. Subsequent D plasmas and operations may have led to additional D retention. Since LIBS only accesses the surface of a PFC we will focus on D retention from DTE3 to the end of operations. The total amount of D injected from the start of DTE3 until the end of operations was 1.55 x 10^{26} D atoms. Assuming a global retention of 0.2 % and a retention fraction of 46.5 % for the inner divertor, we can calculate that 1.44 x 10^{23} D atoms were retained in the inner divertor. Considering the total area of 8.73 m^2 for the inner divertor we determine a D retention of 1.65 x 10^{18} at/cm^2. By applying these calculations, we can determine the T/D ratio to be 0.14 %, significantly higher than the T/D ratio of 0.02 % [24] in the plasma obtained from the neutron data. It is possible that the D retention in this analysis has been underestimated.

The detection limit of D for the Littrow spectrometer was estimated using a reference sample, a 5 µm thick W coating on molybdenum (Mo), exposed to D plasma in the linear plasma device PSI-2. The amount of D (2 at.%) was measured with Nuclear Reaction Analysis (NRA). The detection limit for LIBS was estimated to be 0.07 at.% which corresponds to ~9 x 10^{15} at/cm^2. Assuming the same detection limit for T, the amount of retained T appears to be just below the detection limit in most areas. However, it should be noted that all the numbers provided in Table 3 are only estimations. Confirmation of the actual retained T amounts will be obtained later once the JET tiles are available for post-mortem analyses.

3.2 Comparison of LIBS and SIMS depth profiles

The primary material migration mechanism in JET is Be erosion in the main chamber caused by charge exchange neutrals at the first wall during divertor plasma configurations followed by transport in the scrape-off layer (SOL) to the divertor. Post-mortem results indicate that the upper inner divertor is the area of highest deposition and the dominant region for fuel retention with co-deposits reaching a thickness of up to ~30 µm after exposure for three campaigns. This surface is located in the SOL, does not undergo strong plasma interaction and generally does not exceed surface temperatures of 300 °C. Therefore, material deposited in this region is not eroded and fuel is not desorbed.

Figure 8 shows LIBS and SIMS depth profiles from the horisontal part of tile 1 measured at VTT. The analyses were made on adjacent samples. To construct the depth profiles, the intensities of several lines were summed up to improve the signal to noise ratio [37]. Signal intensities for H(D), Be, Ni, Mo and W are shown in Figure 8. Both depth profiles show the Be co-deposited layer with retained hydrogen isotopes, underlying W layer and finally the Mo interlayer. Due to significant variations in ablation rates between different materials, it is not possible to establish an absolute depth axis for LIBS data by solely measuring crater depth using surface profilometry [38]. In contrast, SIMS exhibits much less variance in sputtering rates across different materials allowing for absolute depth analysis with the help of profilometry. According to SIMS the Be co-deposited layer has a thickness of ~28 µm. In LIBS analyses the number of laser shots required to ablate through the co-deposited layer ranged from 15 to 480 depending on the location on the sample. In Figure 8 (a) the interface is located at ~400. Qualitatively, the agreement between LIBS and SIMS is good in Figure 8.

In Reference [37] several LIBS and SIMS depth profiles from different divertor tiles were compared. Despite some unknown LIBS parameters (such as electron temperature and density)

and a Gaussian laser beam causing uneven ablation of the crater bottom the comparison between LIBS and SIMS provides valuable information on the resolution and accuracy of LIBS for measuring composition and depth profiles.

The feasibility of LIBS in detecting ITER-relevant deposited layers and fuel retention was studied by conducting LIBS measurements on a set of samples from the inner divertor tiles of the ITER-like wall at JET using a ns-laser [38,39]. The results were then compared to those obtained from neighbouring samples using SIMS. The depth profiles detected by LIBS were found to qualitatively agree with those provided by SIMS when the LIBS profiles were scaled with ablation rates. This was achieved by fitting the LIBS data to the SIMS data within each layer until the depth profiles matched those given by SIMS. Therefore, LIBS shows promise as an *in-situ* replacement for post-mortem methods in monitoring metallic co-deposited layers and fuel retention, despite the rather large ablation rates for the thickest layers. The depth resolution of LIBS can be improved by reducing the fluence of the laser beam. This, in practice, involves shortening the laser pulse to the femto/picosecond regime as demonstrated in Reference [40].

3.3 JET LIBS results for WPL limiter

Both the inner wall and outer wall limiters were most extensively analysed during the LIBS experiment (see Table 2). Typically, the tiles have shown erosion in the centre part of the tile [41,42]. The centre region was neighboured by some co-deposition of Be in the far ends of the WPL tiles. Figure 9 shows the analysed tiles on the wide poloidal limiter beam 4D, and in Figure 10, an Aryelle and Littrow spectrum from the centre of the WPL tile 4D14 is presented. The Aryelle spectrum in Figure 10 (a) has several Be peaks at 313.0, 332.2 and 457.3 nm. The most intense Be peak at 465.3 nm is a “ghost“ peak which is an artifact caused during the process of compiling the spectrum in an Echelle-type spectrometer. The Aryelle spectrum also has an H_α peak at 656.3 nm but the resolution of the spectrometer is not high enough to separate the H_α and the D_α components from each other. The wavelength separation of these components is 0.18 nm. Figure 10 (b) shows the Littrow spectrum for the same location. The H_α and the D_α components are only partially separated from each other. The main mechanism of broadening of hydrogenic spectral lines is Stark broadening. Typically, a compromise is made to ensure that both the Stark broadening has decreased sufficiently, and the signal-to-noise (S/N) ratio is still high enough as the emission has not yet faded [43]. In the case of Figure 10 (b) a delay of 8 µs was used. With longer delay times the FWHM of the H_α peak decreases, but it is still ~0.1 nm at 18 µs which is still higher than the gap between the D_α and T_α components (D_α -T_α 0.06 nm)

[43]. The H_α peak appears to be much stronger than the D_α peak which will be discussed in the following chapter.

3.4 JET LIBS results for divertor

Most of the global fuel retention (46.5%) is located in the inner divertor, primarily in co-deposits on tile 0 and tile 1, while the outer divertor accounts for 13.4% of the global retention [37]. Figure 6 displays the analysed locations in divertor module 14. An elemental map of Be and hydrogen isotopes measured with the Aryelle spectrometer is shown in Figure 11 clearly demonstrating the established migration pattern at JET. In few cases more than 1000 laser pulses were applied. In the case of the Be map the Be I lines at 332.1 and 457.3 nm were included. The intensities were normalised to the maximum intensity of the analysed divertor samples [44]. The elemental maps clearly show that D is co-deposited together with Be.

The high-resolution Littrow spectrometer was used to detect hydrogen isotopes. Figure 12 shows a spectrum obtained from divertor tile 23BN G4C. The H_α and D_α components are clearly distinguishable, but due to the Stark broadening, the T_α component cannot be completely separated from the D_α peak. The hydrogen isotope peaks were analysed using a Voigt function and the T/D ratio was determined. The analysis results suggest that the T/D ratio is below 10 %. The H_α peak appears to be much stronger than the D_α peak despite the fact that the amount of puffed H during DTE3 was almost 40 times smaller than the puffed D amount. This may be attributed to the presence of H from moisture on the sample surface, even with Ar fluxing inside the cone that was in contact with the analysed surface. LID-QMS analyses also indicate that the contribution of the HD molecule (mass 3 amu) in the mass spectra is minimal compared to D containing molecules [45]. In Reference [38], LIBS analysis of JET divertor samples was conducted under vacuum conditions, revealing that the D_α peak was notably more intense than the H_α peak. Therefore, it is probable that the prominent H_α peak in Figures 10 and 12 is at least partly due to air contamination and does not accurately represent the actual H content in the tiles.

Elemental maps for D/H and T/H ratios were also generated, as shown in Figure 13. The results are displayed only for the first 100 laser pulses. Littrow results also indicate that the heaviest deposition is on tiles 0 and 1 with D present on outer divertor tile 8. The T/H map (see Figure 13 (c)) reveals that the amount of T on the divertor tiles is very small consistent with observations in the Littrow spectrum in Figure 12. Neutron data for the T/D ratio from 14 MeV (DT) and 2.4 MeV (DD) neutron production during the clean-up campaign indicated a reduction by two orders of magnitude. Therefore, it is evident that the T signal in the LIBS data is low.

3.5 Inconel wall

Six locations on the Inconel vessel wall were analysed with LIBS for fuel retention. Analysis of the vessel wall has not been possible before with any post-mortem analysis technique used in the analysis of JET PFCs. Figure 14 (a) shows the LIBS locations on the vessel wall in Octant 1. Figure 14 (b) presents the spectrum measured with the Aryelle spectrometer. In addition to Ni I, Fe I and Cr I peaks, the spectrum also has Be I, Be II and H_α lines. The co-deposited layer on the vessel wall is thin because only six laser pulses were required to ablate through it. The spectrum measured from the vessel wall with the Littrow spectrometer is shown in Figure 14 (c). D_α and H_α peaks are nicely separated from each other, and the peak width (FWHM) is actually narrower than in, for example, Figure 10 (b) and 12, but only for the first three laser pulses. For subsequent laser pulses the D_α and H_α peaks are wider.

4. Conclusions

As a licensed nuclear facility, ITER must limit the in-vessel tritium (T) retention to reduce the risks of potential release during accidents, with the maximum retention in the in-vessel components set at 700 g. Therefore, the analysis of the retention of nuclear fuel is crucial for ITER and future nuclear fusion devices like DEMO. Among the possible *in-situ* techniques, laser-based techniques, such as LIBS and LID-QMS, are promising candidates for first wall characterisation of a fusion device providing in-vessel local fuel retention measurements for comparison with global fuel retention and with ex-vessel post-mortem measurements on retrieved PFCs.

A novel LIBS system was developed at ENEA and optimised by Forschungszentrum Jülich. Prior to the actual LIBS experiment at JET comprehensive test and calibration measurements were conducted at VTT using JET samples cut from PFCs removed during the 2016 shutdown. Optimal experimental conditions including studies of gate width of the Aryelle spectrometer and delay between the laser pulse and acquisition were established. LIBS depth profiles were acquired for JET divertor and limiter samples exposed in the 2011–2016 campaigns at various locations across the vacuum vessel and compared with SIMS depth profiles. Despite some unknown LIBS parameters, such as electron temperature and density, and the Gaussian laser beam causing uneven ablation of the crater bottom the comparison between LIBS and SIMS provides useful information on the resolution and accuracy of LIBS for measuring composition

and depth profiles. LIBS results confirm the erosion and deposition pattern observed earlier in post-mortem analyses.

Further test measurements were performed at UKAEA to optimise the quality of the laser beam and improve the sensitivity of the LIBS system. Subsequently, the LIBS hardware was relocated from the optical lab at UKAEA to the JET torus hall and commissioned within the controlled area. Final calibration measurements were performed using H/D, D, Hg and W lamps for wavelength calibration as well as an Ulbricht sphere for radiometric calibration. The LIBS tool was mounted on the MASCOT arms. The actual LIBS experimental campaign at JET using remote handling was successfully carried out between the 2nd and 18th of October in double shifts. 840 different spatial locations on the main wall and divertor area were investigated, with measurements of more than 100 laser pulses per location executed to ensure good depth resolution. In total, ~323000 laser shots were applied each producing an Aryelle, Littrow and Avantes spectrum. The amount of data generated is substantial so advanced Matlab and machine learning algorithms will be utilised for batch processing of the spectra during the data analysis. Machine learning will involve removing redundant data, detecting anomalies, extracting features, reducing dimensionality and ultimately estimating quantitative chemical contents.

Only the Littrow spectrometer used during the LIBS experiments at JET was capable of resolving the hydrogen-alpha line into isotopic peaks whereas the resolution of the Aryelle and Avantes spectrometers was insufficient. The H_α and D_α components were only partially separated from each other due to Stark broadening. A compromise was selected to decrease the Stark broadening sufficiently while maintaining a high enough S/N ratio since the emission had not yet faded away. The hydrogen isotope peaks were analysed using a Voigt function and the T/D ratio was determined. The LIBS measurements were conducted after a thorough tritium clean-up campaign, leading to a significant reduction in tritium levels. The concentration of tritium was too low to be detected and measured by LIBS in the majority of the areas analysed.

Acknowledgements

This work has been carried out within the framework of the EUROfusion Consortium, funded by the European Union via the Euratom Research and Training Programme (Grant Agreement No 101052200 — EUROfusion), from the EPSRC [grant number EP/W006839/1] and within the framework of the Contract for the Operation of the JET Facilities and has received funding from the European Union's Horizon 2020 research and innovation programme. Views and opinions expressed are however those of the author(s) only and do not necessarily reflect those of the European Union or the European Commission. Neither the European Union nor the

European Commission can be held responsible for them. The research used UKAEA's Materials Research Facility, which has been funded by and is part of the UK's National Nuclear User Facility and Henry Royce Institute for Advanced Materials.

References

[1] J. Roth, E. Tsitrone, Th. Loarer, et el., Plasma Phys. Control. Fusion 50 (2008) 103001.

[2] R. Reichle, P. Andrew, P. Bates et al., J. Nucl. Mater. 463 (2015) 180.

[3] D.A. Cremers and L.J. Radziemski, Handbook of Laser-Induced Breakdown Spectroscopy, Wiley, 2006.

[4] D.D.R. Summers, M.N.A. Beurskens, J.P. Coad, et al., J. Nucl. Mater.290-293 (2001) 496.

[5] C. Grisolia, A. Semerok, J. M. Weulersse, et al., J. Nucl. Mater. 363-365 (2007) 1138.

[6] A. Semerok, D. L'Hermite, J.-M. Weulersse, et al. Spectrochim. Acta part B 123 (2016) 121.

[7] B. Schweer, G. Beyene, S. Brezinsek, et al., Phys. Scr. T138 (2009) 014008.

[8] A. Huber, B. Schweer, V. Philipps, et al., Fusion Eng. Des. 86 (2011) 1336.

[9] Q. Xiao, R. Hai, H. Ding, A. Huber, V. Philipps, N. Gierse, G. Sergienko, J. Nucl. Mater.463 (2015) 911.

[10] S. Almaviva, L. Caneve, F. Colao and G. Maddaluno, Phys. Scr. 91 (2016) 044003.

[11] G. Maddalunoa, S. Almavivaa, L. Caneve, et al., Nucl Mater. Energy 18 (2019) 208.

[12] S. Almaviva, L. Caneve, F. Colao, et al., Fusion Eng. Des. 157 (2020) 111685.

[13] S. Almaviva, L. Caneve, F. Colao, et al., Fusion Eng. Des. 169 (2021) 112638.

[14] D. Zhao, C. Li, Y. Wang, et al., Plasma Sci. Technol. 20 (2018) 014022.

[15] P. Liu, R. Hai, D. Wu, Q. Xiao, L. Sun, and H. Ding, Plasma Sci. Technol. 17 (2015) 687.

[16] R. Hai, N. Farid, D. Zhao, L. Zhang, J. Liu, H. Ding, J.Wu, and G.-N. Luo, Spectrochim. Acta, Part B 87 (2013) 147.

[17] R. Hai, X.Wu, Y. Xin, et al., J. Nucl. Mater. 447 (2014) 9.

[18] C. Li, D. Zhao, X. Wu, and H. Ding, Plasma Sci. Technol. 17 (2015) 638.

[19] D. Zhao, N. Gierse, J. Wegner, et al., Nucl. Instrum. Methods Phys. Res., Sect. B 418 (2018) 54.

[20] H. Y. Oderji, N. Farid, L. Sun, C. Fu, and H. Ding, Spectrochim. Acta, Part B 122 (2016) 1.

[21] Z. Hu, C. Li, Q. Xiao, et al., Plasma Sci. Technol. 19 (2017) 025502.

[22] Z. Hu, X. Bai, H. Wu, et al., Nucl Mater. Energy 41 (2024) 101785.

[23] A. Favre, A. Bultel, M. Lamine Sankheet al., Phys. Scr. 99 (2024) 035609.

[24] A. Widdowson, S. Brezinsek, T. Dittmar, et al., submitted Nucl. Fusion.

[25] G. S. Maurya, A. Marín-Roldán, P. Veis, A. K. Pathak, and P. Sen, J. of Nucl. Mater., 541 (2020) 152417.

[26] S. Atikukke, P.G Bhat, I. Urbina, G.S , Maurya and P. Veis (2025). Application of LIBS in Nuclear Technology. In G. Galbács (Ed.), Laser Induced Breakdown Spectroscopy in Biological, Forensic and Materials Sciences (pp. 507–536). Springer, Cham.

[27] H. J. van der Meiden, S. Almaviva, J. Butikova et al., Nucl. Fusion, 61 (2021) 125001.

[28] P. Gąsior, ACTA PHYSICA POLONICA A 138 (2020) 601.

[29] ZEMAX Optical Design Software: https://www.ansys.com/products/optics/ansys-zemax-opticstudio.

[30] J. Likonen, S. Lehto, J.P. Coad et al., Fus. Eng. Design 66-68 (2003) 219.

[31] A. Widdowson, A. Baron-Wiechec, P. Batistoni et al., Phys. Scr. T167 (2016) 014057.

[32] D. Matveev, D. Douai, T. Wauters et al., Nucl. Fusion 63 (2023) 112014.

[33] C.F. Maggi, D. Abate, N. Abid et al., Nucl. Fusion 64 (2024) 112012.

[34] X. Jiang, G. Sergienko, A. Kreter, S. Brezinsek and Ch. Linsmeier, Nucl. Fusion 61 (2021) 096006.

[35] D. Hamilton and G. Preece, Development of the MASCOT Telemanipulator Control System, EFDA–JET–PR(01)06 report.

[36] A. Widdowson, J.P. Coad, Y. Zayachuk et al., Phys. Scr. 96 (2021) 124075.

[37] J. Ristkok, S. Almaviva, J. Likonen et al., Nucl Mater. Energy to be published.

[38] J. Karhunen, A. Hakola, J. Likonen et al., J. Nucl. Materials 463 (2015) 931.

[39] J. Karhunen, A. Hakola, J. Likonen et al., Phys. Scr. T159 (2014) 014067.

[40] E. Wüst, T. Schwarz-Selinger, C. Kawan, et al. Phys Plasmas, 31 (2024) 082510.

[41] K. Heinola, A. Widdowson, J. Likonen et al., J. Nucl. Mater. 463 (2015) 961.

[42] Y. Zayachuk, N. Catarino, J. Likonen, M. Rubel and A. Widdowson, Nucl Mater. Energy 42 (2025) 101872.

[43] R. Yi, R. Rayaprolu, J. Likonen et al. this conference.

[44] S. Almaviva, J. Likonen, A. Hakola et al. this conference.

[45] M. Zlobinski, G. Sergienko, I. Jepu et al., Nucl. Fusion 64 (2024) 086031.

Tables

Table 1. List of analysed samples.

Sample	**Location**	**Layers**	Exposure period
HFGC_3c	Tile 0	CFC, Mo, W	ILW 1-3
HFGC_1c	Tile 0	CFC, Mo, W	ILW 1-3
14IWG1A_12a	Tile 1 apron	CFC, Mo, W	ILW 1-3
14IWG1A_11a	Tile 1 apron	CFC, Mo, W	ILW 1-3
14IWG1A_8a	Tile 1 diagonal	CFC, Mo, W	ILW 1-3
14IWG1A_3a	Tile 1 vertical	CFC, Mo, W	ILW 1-3
2IWG3A_6a	Tile 3	CFC, Mo, W	ILW 3
B12_167	Tile 5	W lamella	ILW 1,3
2ONG7A_7	Tile 7	CFC, Mo, W	ILW 2-3
2ONG8B_7b	Tile 8	CFC, Mo, W	ILW 2-3
2ONG8B_11b	Tile 8	CFC, Mo, W	ILW 2-3
2XR11_623	Inner wall limiter	Be	ILW 1-3
2XR11_641	Inner wall limiter	Be	ILW 1-3
2XR11_668	Inner wall limiter	Be	ILW 1-3
4D15_686	Outer poloidal limiter	Be	ILW 1-3
4D15_703	Outer poloidal limiter	Be	ILW 1-3
IWC_2	Inner vessel wall	Be, Inconel (Ni, Fe, Cr)	Not exposed

Table 2. Number of analysed locations in different areas of the JET vacuum vessel.

Location ID	Number of locations
Inner wall guard limiters (IWGL)	308
Wide poloidal limiters (WPL)	272
Divertor	232
Inner wall protection	22
Vessel wall	6
Total	840

Table 3. Calculated T inventory in PFCs before and after the clean-up campaign.

Plasma facing component	T retention on plasma facing surfaces from post mortem analysis @ 0.19% (not including clean-up) (T atoms/cm^2)	T retention on plasma facing surfaces with T clean-up and vessel venting (T atoms/cm^2)
Inner divertor tiles	4-10 x 10^{17}	4-10 x 10^{15}
Outer divertor tiles	1.5-3 x 10^{17}	1.5-4 x 10^{15}
Beryllium limiter tiles	~1 x 10^{17}	~1 x 10^{15}

Figure Captions

Figure 1. LIBS setup used at VTT.

Figure 2. Analysed samples and locations in the JET vacuum vessel. One non-exposed Be-coated Inconel sample IWC_2 was also measured mimicking inner vessel wall for identifying Inconel spectral lines.

Figure 3. Final LIBS setup at JET.

Figure 4. MASCOT (a) and remote handling boom (b) at JET. LIBS enclosure was mounted onto the MASCOT arm.

Figure 5. Analysed locations (marked with "x") on OPL tile 4D13. Location of tile 4D13 is also shown on the limiter beam.

Figure 6. Analysed locations on the divertor module 14. Not all locations are shown in the figure.

Figure 7. Inner wall protection tile IWP428 with sachet samples.

Figure 8. (a) LIBS depth profile for sample 14IWG1A_11 and (b) SIMS depth profiles for sample 14IWG1A_10a (locations of the samples shown in Figure 2).

Figure 9. (a) WPL limiter beam 4D and analysed tiles, (b) analysis locations on tile 4D14, red circle indicates the analysis location for the spectra shown in Figure 10.

Figure 10. (a) Aryelle and (b) Littrow spectrum measured from centre of limiter tile 4D4.

Figure 11. (a) Be and (b) hydrogen isotope map for divertor module 14 measured with the Aryelle spectrometer. The horisontal axis represents the analysed location at the divertor while the vertical axis represents the number of laser shots applied.

Figure 12. Littrow spectrum measured from tile 23BWG4C showing hydrogen isotope components. Analysis location is shown in the insert.

Figure 13. D/H (B) and T/H (c) elemental maps generated from Littrow results. The locations of the analysis points are shown in (a).

Figure 14. LIBS locations on the vessel wall in Octant 1. Aryelle (b) and Littrow (c) spectrum measured from the centre of the vessel wall.

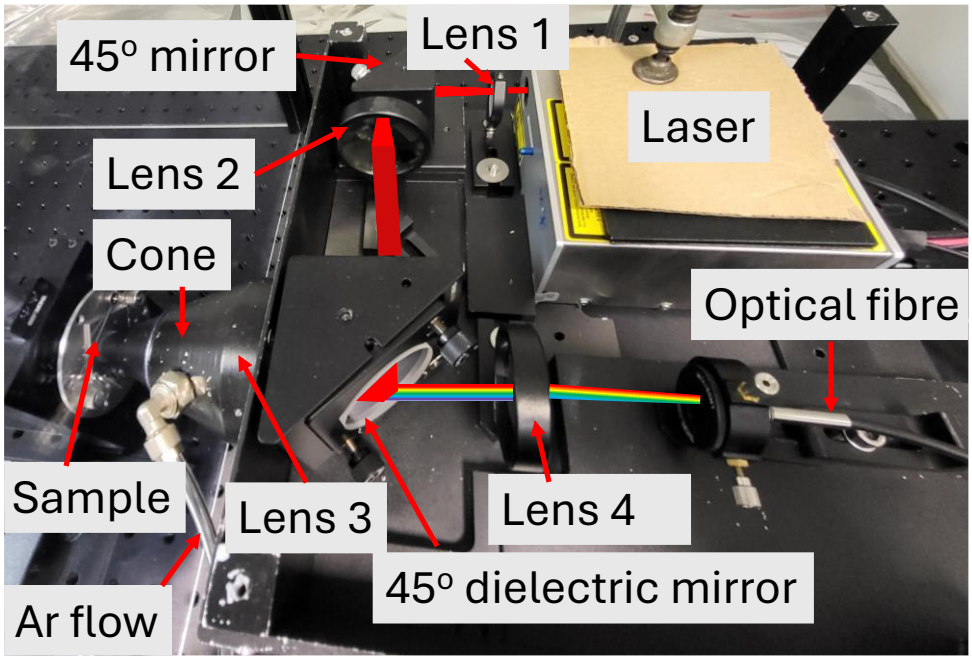
45º mirror
Lens 1
Laser
Lens 2
Cone
Optical fibre
Sample
Lens 3
Lens 4
45º dielectric mirror
Ar flow

Figure 1.

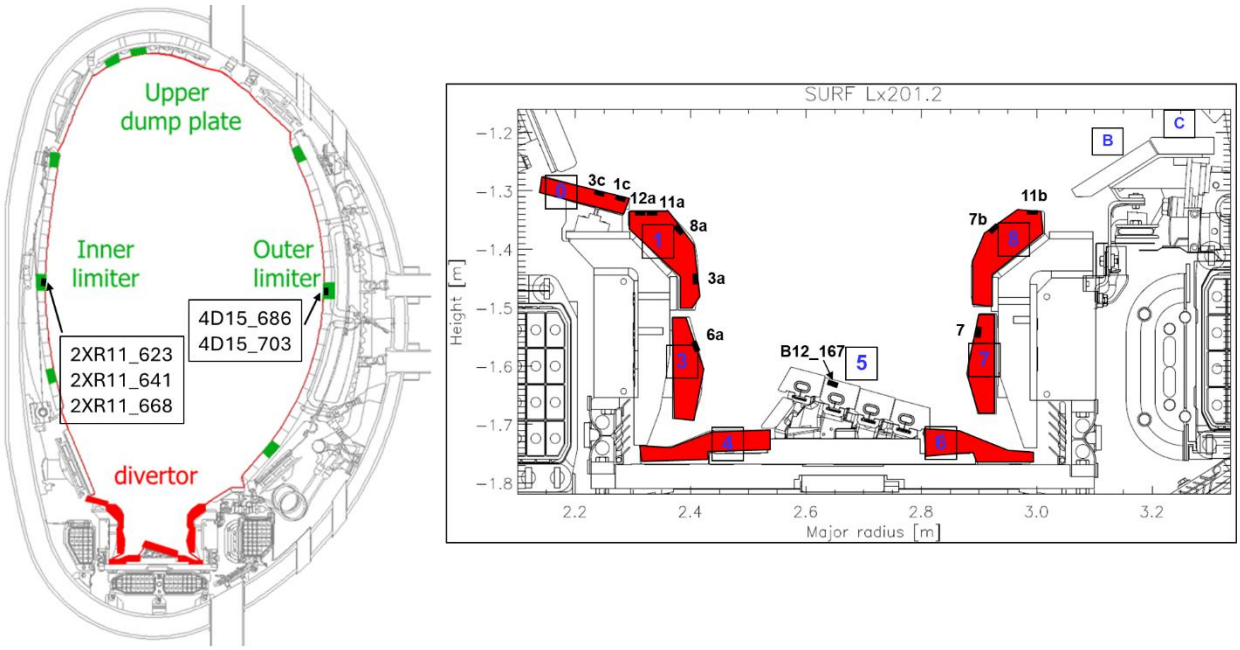
Upper
dump plate
Inner
limiter
Outer
limiter
4D15_686
4D15_703
2XR11_623
2XR11_641
2XR11_668
divertor
SURF Lx201.2
Height [m]
Major radius [m]
3c
1c
12a
11a
8a
3a
6a
B12_167
11b
7b
7
B
C

Figure 2.

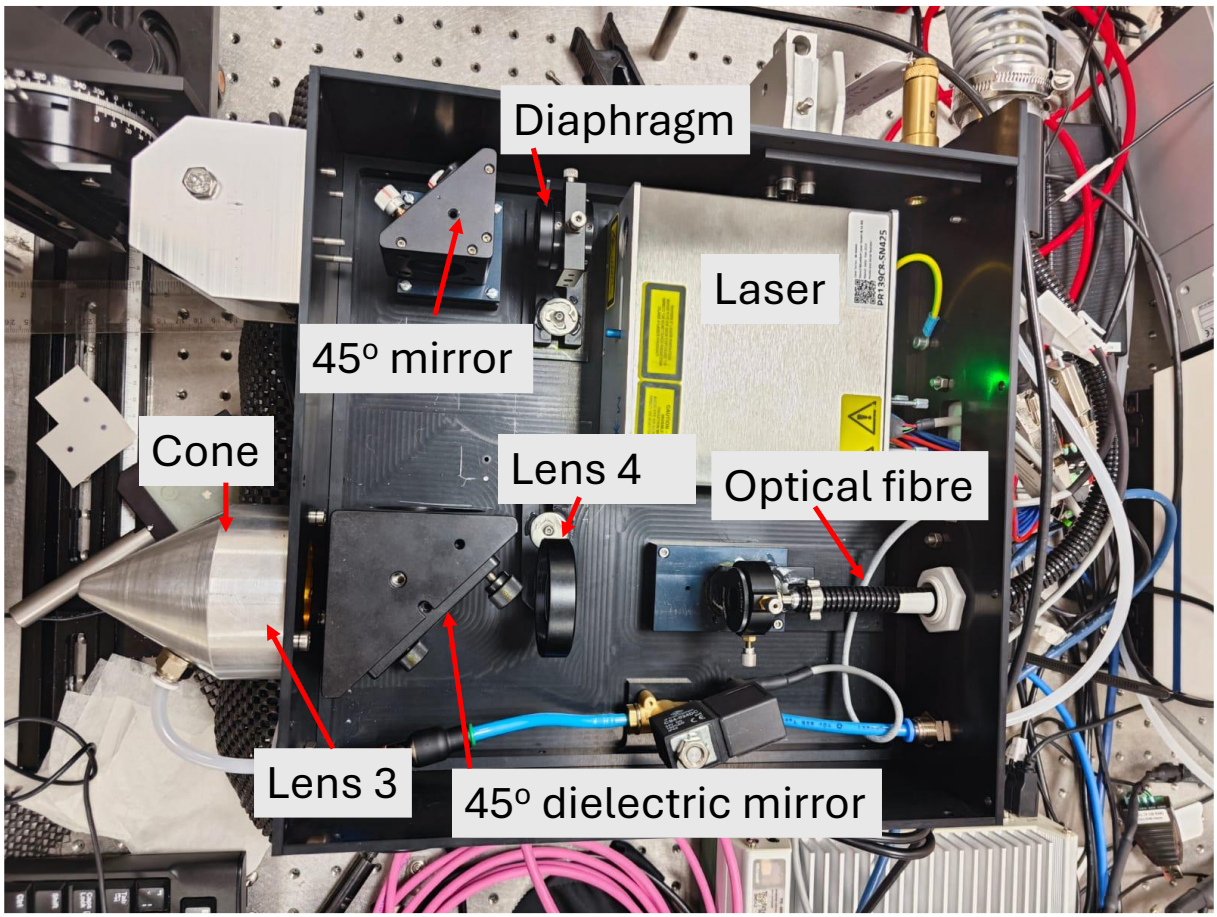
Diaphragm
Laser
45° mirror
Cone
Lens 4
Optical fibre
Lens 3
45° dielectric mirror
Figure 3.

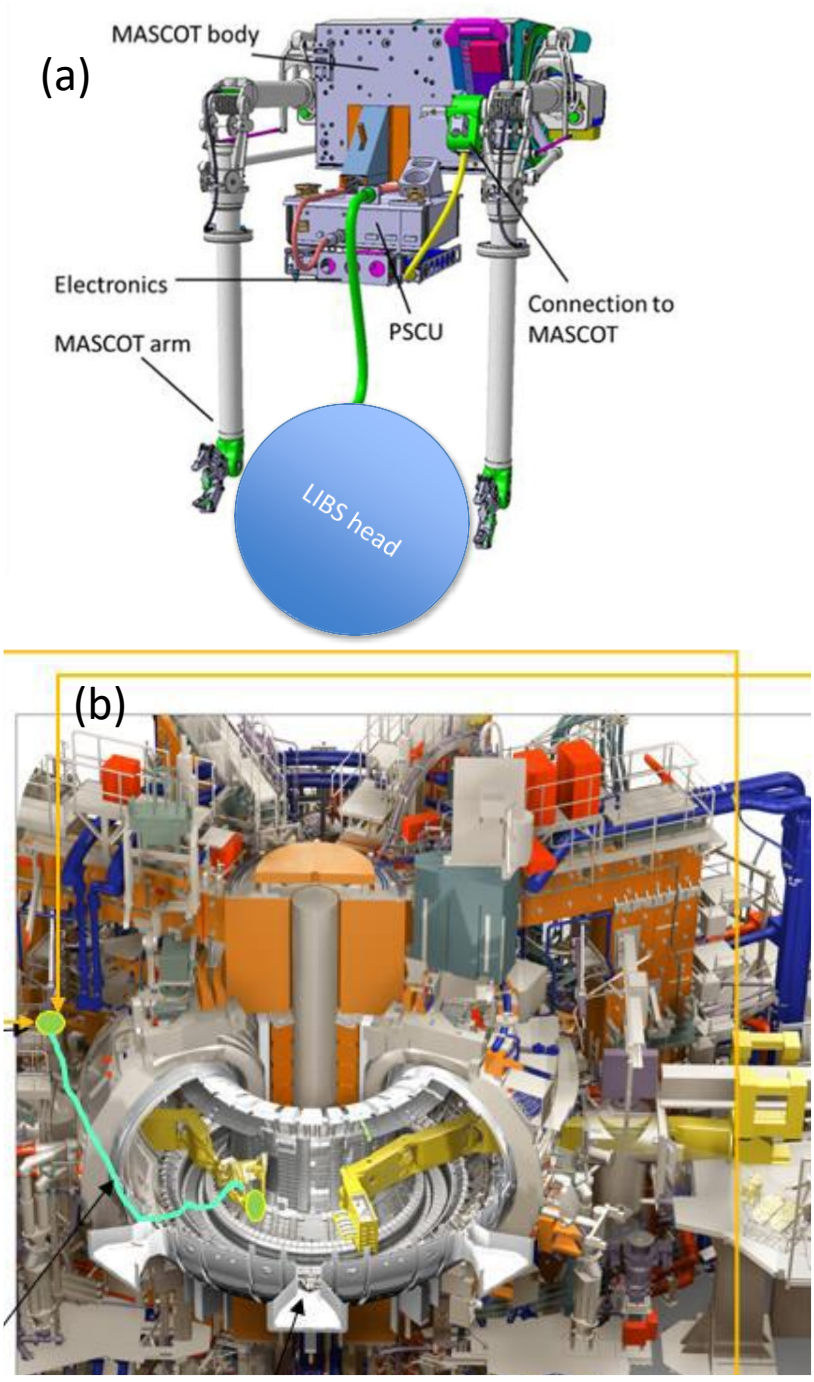
(a)
MASCOT body
Electronics
MASCOT arm
PSCU
Connection to MASCOT
LIBS head
(b)
Figure 4.

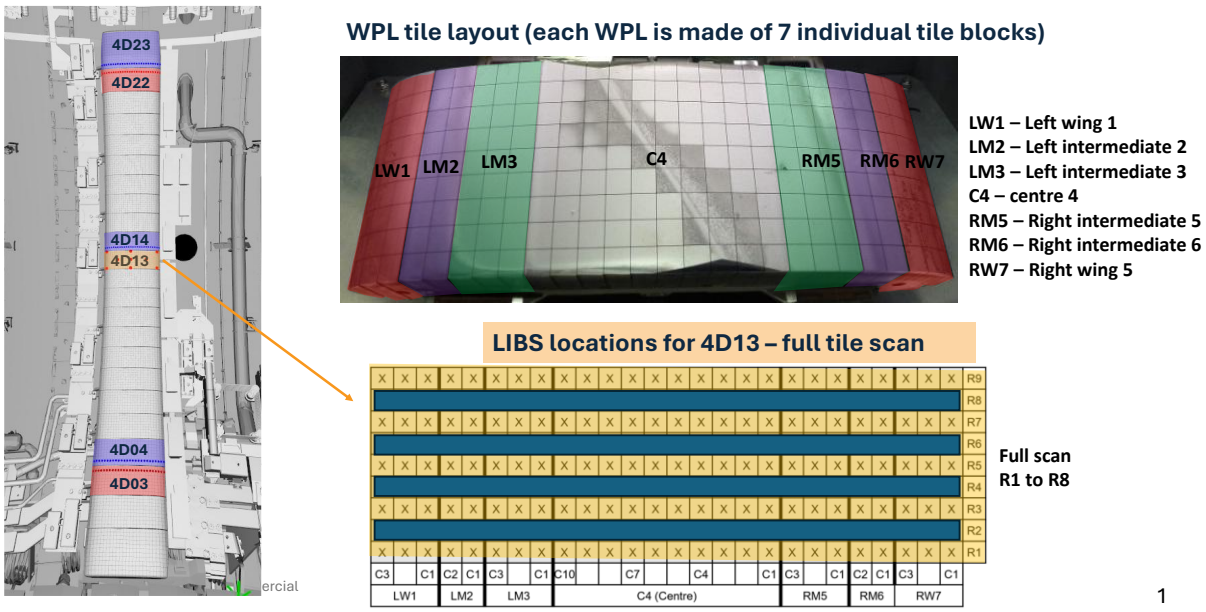
4D23
4D22
4D14
4D13
4D04
4D03
WPL tile layout (each WPL is made of 7 individual tile blocks)
LW1
LM2
LM3
C4
RM5
RM6
RW7
LW1 – Left wing 1
LM2 – Left intermediate 2
LM3 – Left intermediate 3
C4 – centre 4
RM5 – Right intermediate 5
RM6 – Right intermediate 6
RW7 – Right wing 5
LIBS locations for 4D13 – full tile scan
R9
R8
R7
R6
R5
R4
R3
R2
R1
C3 C1 C2 C1 C3 C1 C10 C7 C4 C1 C3 C1 C2 C1 C3 C1
LW1
LM2
LM3
C4 (Centre)
RM5
RM6
RW7
Full scan
R1 to R8

Figure 5.

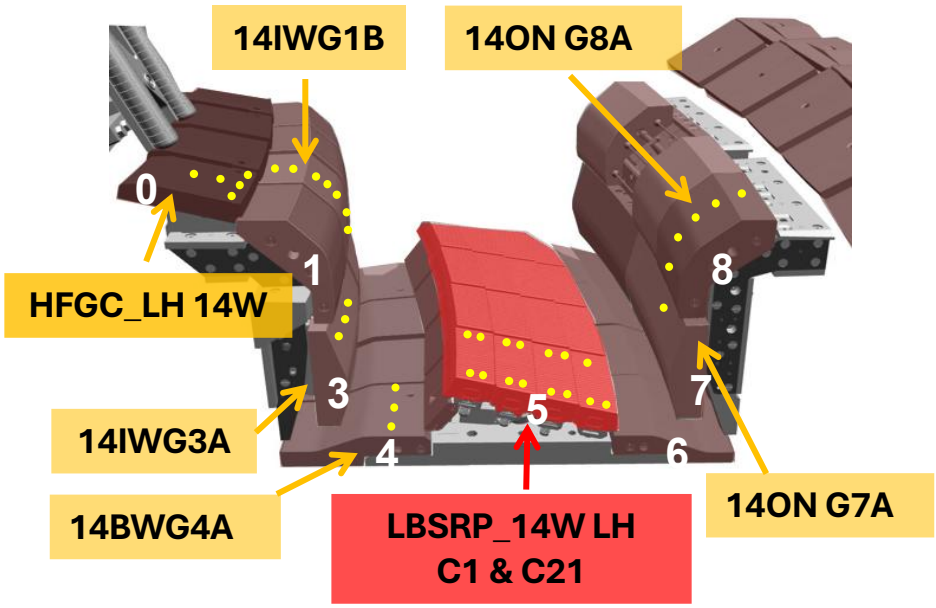
14IWG1B
14ON G8A
0
HFGC_LH 14W
1
8
3
7
5
14IWG3A
4
6
14BWG4A
LBSRP_14W LH
C1 & C21
14ON G7A

Figure 6.

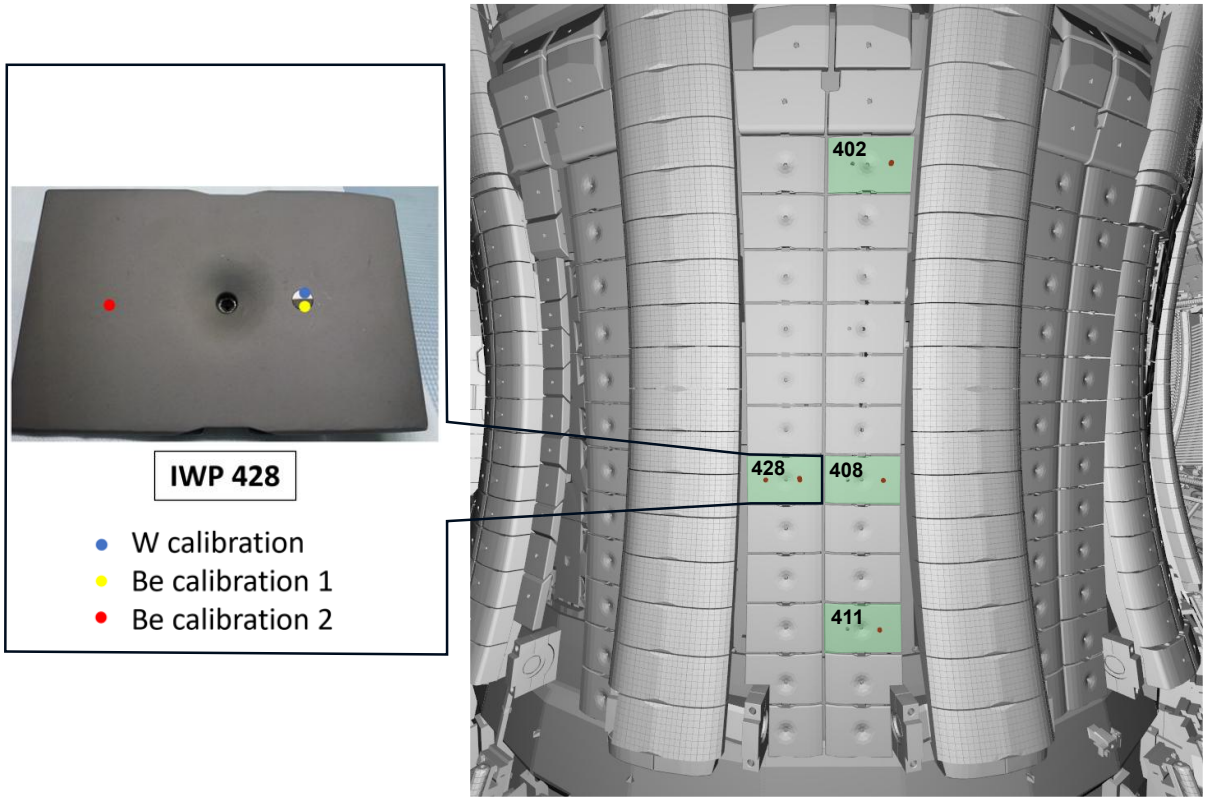
IWP 428
W calibration
Be calibration 1
Be calibration 2
402
428
408
411

Figure 7.

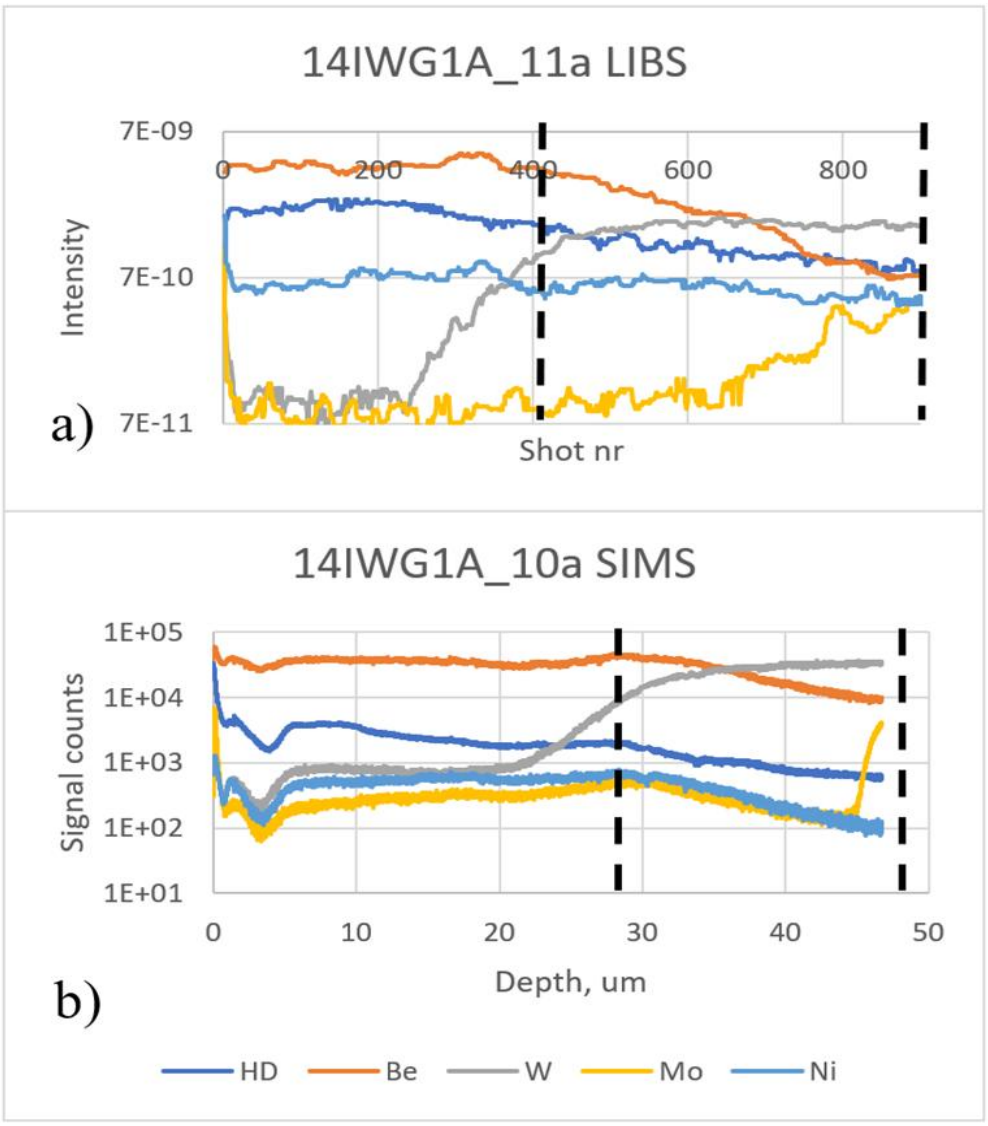
14IWG1A_11a LIBS
7E-09
7E-10
7E-11
Intensity
0
200
400
600
800
Shot nr
a)
14IWG1A_10a SIMS
1E+05
1E+04
1E+03
1E+02
1E+01
Signal counts
0
10
20
30
40
50
Depth, um
b)
HD
Be
W
Mo
Ni

Figure 8.

a)

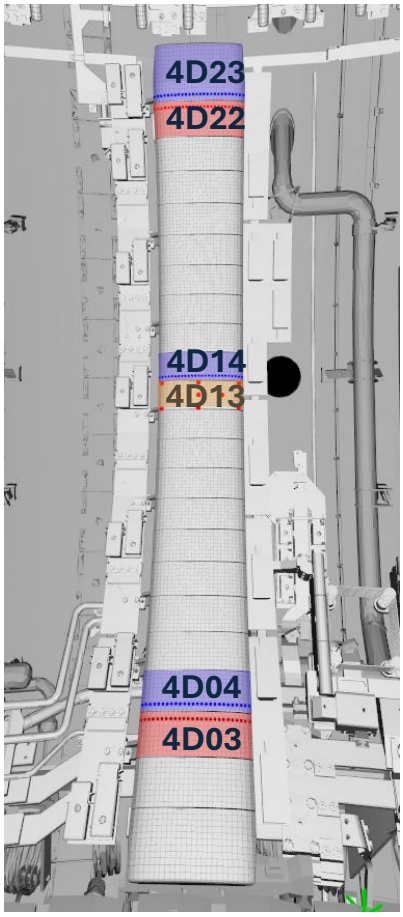
4D23
4D22
4D14
4D13
4D04
4D03

b)

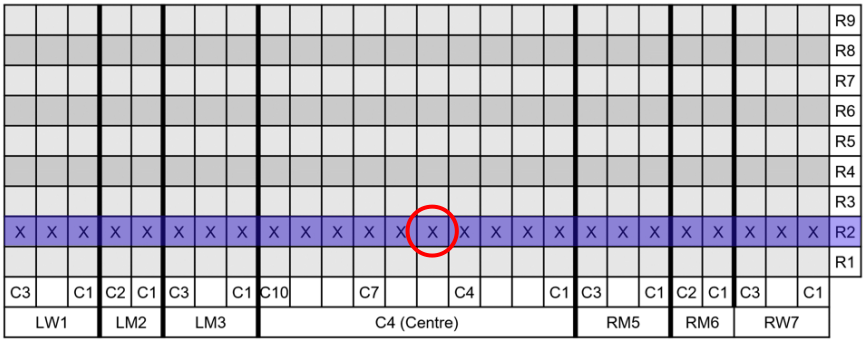
R9
R8
R7
R6
R5
R4
R3
R2
R1
C3 C1 C2 C1 C3 C1 C10 C7 C4 C1 C3 C1 C2 C1 C3 C1
LW1 LM2 LM3 C4 (Centre) RM5 RM6 RW7

Figure 9.

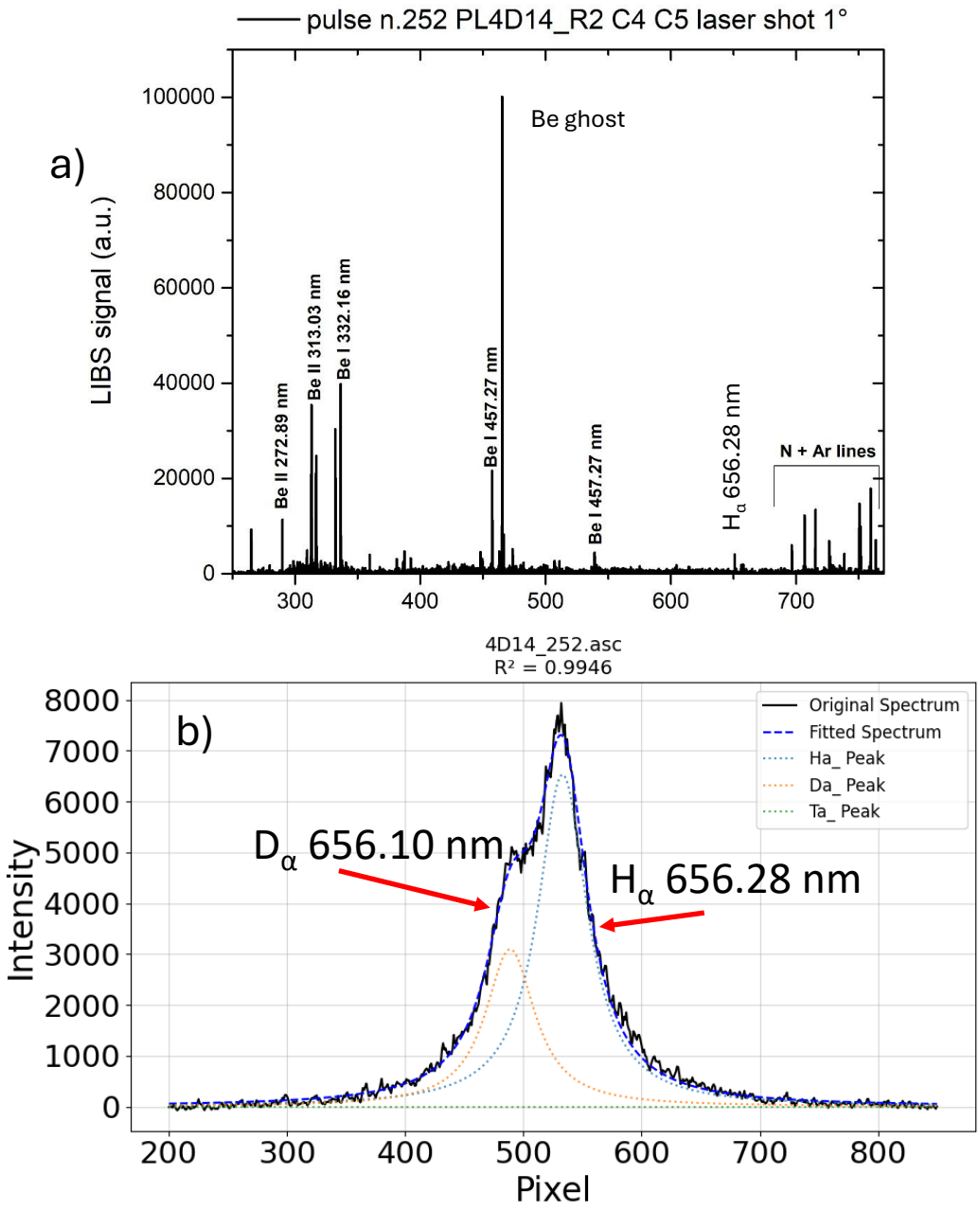
pulse n.252 PL4D14_R2 C4 C5 laser shot 1°
a)
LIBS signal (a.u.)
Be ghost
Be II 272.89 nm
Be II 313.03 nm
Be I 332.16 nm
Be I 457.27 nm
Be I 457.27 nm
Hα 656.28 nm
N + Ar lines
4D14_252.asc
R² = 0.9946
b)
Original Spectrum
Fitted Spectrum
Ha_ Peak
Da_ Peak
Ta_ Peak
Dα 656.10 nm
Hα 656.28 nm
Intensity
Pixel

Figure 10.

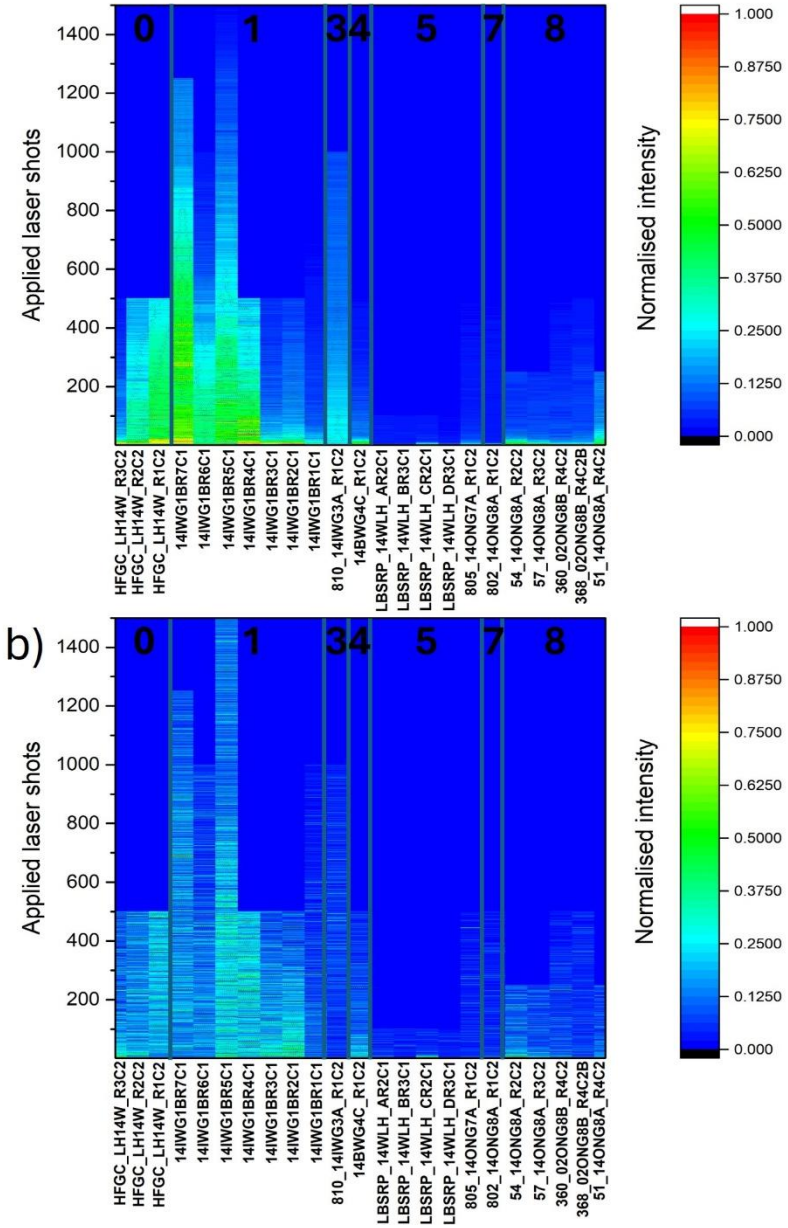
b)
0
1
34
5
7
8
Applied laser shots
1400
1200
1000
800
600
400
200
Normalised intensity
1.000
0.8750
0.7500
0.6250
0.5000
0.3750
0.2500
0.1250
0.000
HFGC_LH14W_R3C2
HFGC_LH14W_R2C2
HFGC_LH14W_R1C2
14IWG1BR7C1
14IWG1BR6C1
14IWG1BR5C1
14IWG1BR4C1
14IWG1BR3C1
14IWG1BR2C1
14IWG1BR1C1
810_14IWG3A_R1C2
14BWG4C_R1C2
LBSRP_14WLH_AR2C1
LBSRP_14WLH_BR3C1
LBSRP_14WLH_CR2C1
LBSRP_14WLH_DR3C1
805_14ONG7A_R1C2
802_14ONG8A_R1C2
54_14ONG8A_R2C2
57_14ONG8A_R3C2
360_02ONG8B_R4C2
368_02ONG8B_R4C2B
51_14ONG8A_R4C2

Figure 11.

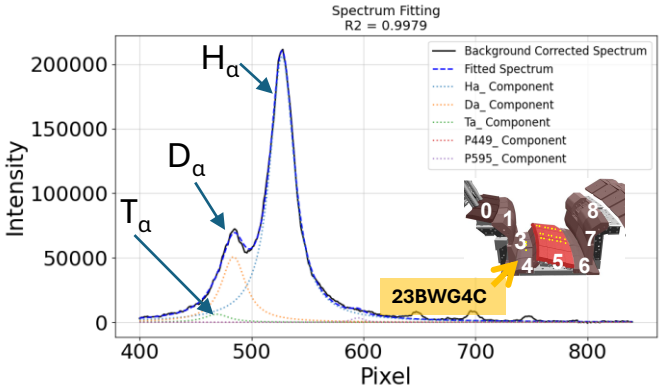
Spectrum Fitting
R2 = 0.9979
Background Corrected Spectrum
Fitted Spectrum
Ha_ Component
Da_ Component
Ta_ Component
P449_ Component
P595_ Component
Hα
Dα
Tα
Intensity
Pixel
200000
150000
100000
50000
0
400
500
600
700
800
0
1
3
4
5
6
7
8
23BWG4C

Figure 12.

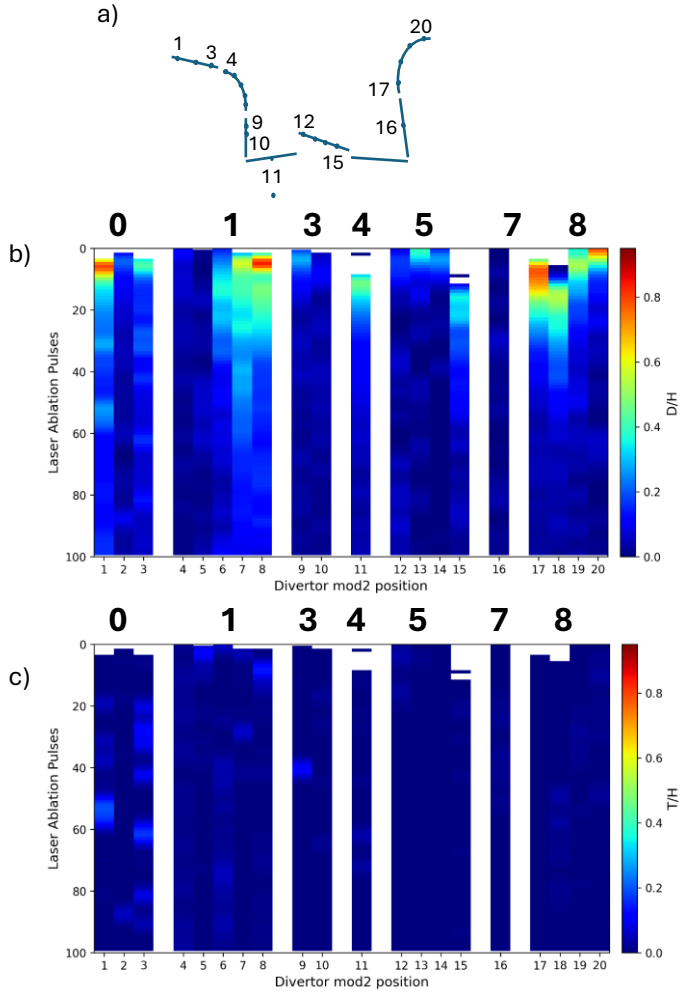
a)
1
3
4
9
10
11
12
15
16
17
20
b)
0
1
3
4
5
7
8
Laser Ablation Pulses
Divertor mod2 position
D/H
c)
T/H

Figure 13.

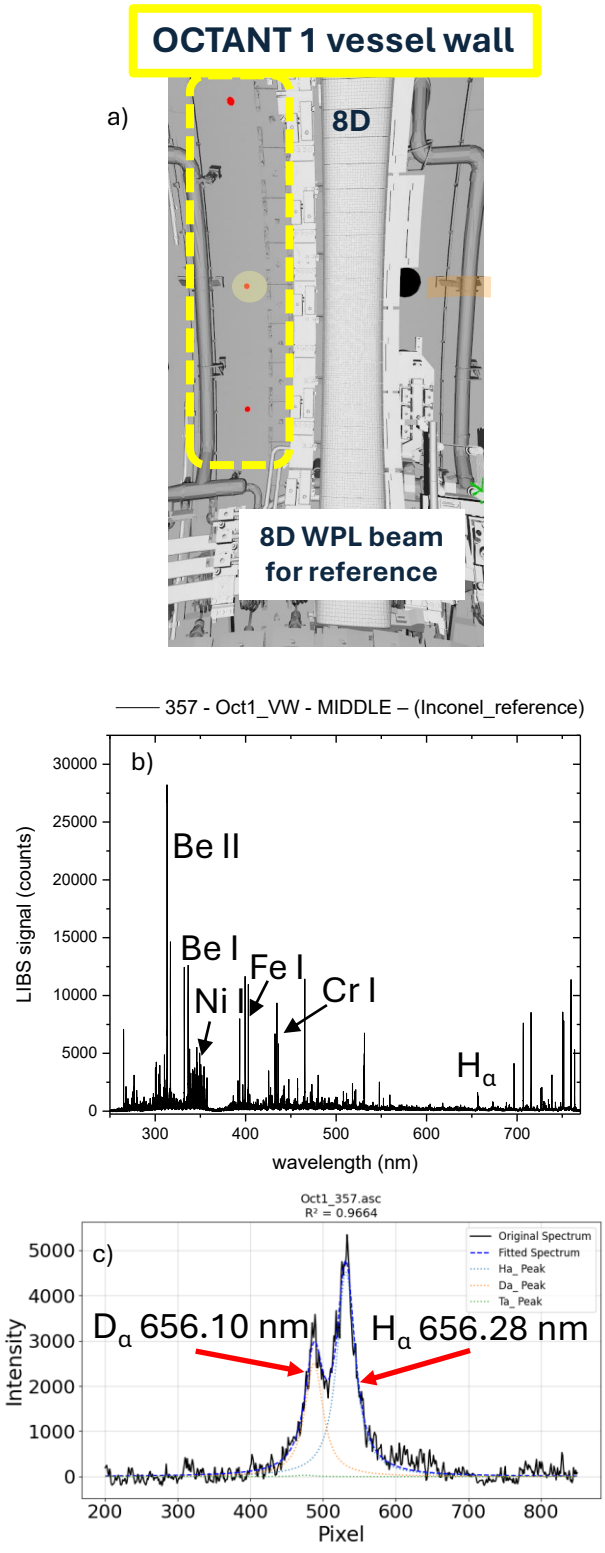
OCTANT 1 vessel wall
a)
8D
8D WPL beam for reference
357 - Oct1_VW - MIDDLE – (Inconel_reference)
b)
Be II
Be I
Ni I
Fe I
Cr I
H_α
LIBS signal (counts)
wavelength (nm)
Oct1_357.asc
R² = 0.9664
c)
Original Spectrum
Fitted Spectrum
Ha_ Peak
Da_ Peak
Ta_ Peak
D_α 656.10 nm
H_α 656.28 nm
Intensity
Pixel

Figure 14.